IEEE Access
Multidisciplinary | Rapid Review | Open Access Journal

Received July 22, 2018, accepted August 20, 2018, date of publication August 23, 2018, date of current version September 21, 2018.

Digital Object Identifier 10.1109/ACCESS.2018.2866862

Calculation of Lightning Induced Overvoltages on Overhead Lines: Model and Interface With MATLAB/Simulink

XIN LIU, ZIWEI FAN, GUISHU LIANG, AND TAO WANG
Department of Electrical Engineering, North China Electric Power University, Baoding 071003, China

Corresponding author: Xin Liu (liuxinhust@163.com)

This work was supported in part by the Fundamental Research Funds for the Central Universities under Grant 2017MS100 and in part by the National Natural Science Foundation of China under Grant 51407073.

ABSTRACT This paper presents a macro-model, which can be used to calculate the lightning-induced overvoltages (LIOVs) on overhead lines on MATLAB/Simulink platform. First, a macro-model according to Agrawal's field-to-line coupling model is derived, in which the distributed equivalent voltage sources due to the horizontal components of the incident electric fields are lumped at the terminals of the transmission lines. In order to interface with MATLAB/Simulink, the propagation function of the transmission line is approximated by a delayed rational function and described by a state-space representation, and Brune's synthesis is adopted to model the equivalent multiport equivalent circuit of the transmission line in order to overcome the passivity violation problem. Combining with the built-in components in MATLAB/Simulink, the proposed modeling approach is applied to evaluate LIOVs of an overhead lines system, and the influence of the arrester and ground wire on the LIOVs is discussed in this paper. Furthermore, considering that the peak values of LIOVs are mainly concerned in the insulation coordination, a simple model for the early time response is proposed, which can further simplify the procedure. The accuracy of the proposed modeling method is validated by some examples.

INDEX TERMS Multi-conductor transmission lines, lightning induced overvoltages, Brune's synthesis, MATLAB/Simulink.

I. INTRODUCTION

It is essential to estimate the overvoltages of multi-conductor transmission lines (MTLs) induced by external electromagnetic (EM) fields [1]. Many methods are available to analyze this problem [2]–[22]. Among these methods, the full-wave model is supposed to be the most accurate one [2], because it is based on the Maxwell's equations. However, because the variables are the electric and the magnetic fields, it could not be directly applied to analyze a complex network composed of lumped elements, especially when some nonlinear components are included [3]. Compared with the full-wave method, the field-to-line coupling model is an attractive choice due to its sufficient efficiency and accuracy [4]. It is well known that the Agrawal's field-to-line coupling model is one of the most widespread models used to evaluate the lightning induced overvoltage (LIOV) of transmission lines. The famous Baum-Liu-Tesche (BLT) formulation [5] provides a general solution of the Agrawal's field-to-line coupling model, however, it is difficult to treat the nonlinear problems since it is mainly implemented in the frequency domain [6], [7]. Time domain finite element method (TDFEM) [3] and finite difference time domain (FDTD) [8], [9] are two time domain methods to solve the Agrawal's filed-to-line coupling model by using time and spatial discretization schemes, which have been widely used to evaluate LIOV. Especially, a simple and fast computer code with only 300 lines written in Matlab has been developed by Barbosa and Paulino based on finite difference time domain technique [10], [11], which simplifies the procedure to evaluate LIOV. On the other hand, lots of work has been done to develop some circuit simulator compatible models, because they can be directly integrated into circuit simulators, such as EMTP-RV, ATP, PSPICE, MATLAB/Simulink, PSCAD, etc., to analyze the effects produced by indirect lightning on distributed overhead line networks of any complexity in terms of dimensions and variety of components.

Montaño *et al*. proposed a PSPICE compatible model by dividing the transmission lines into a series of segments and

the coupling mechanisms are represented by some distributed sources due to the horizontal components of the incident electric fields [12]. However, as for a complex power network or a line several kilometers long, a large number of segments are required to achieve accurate results. It can be imagined that the implementation procedure is somewhat complicated, since inserting the distributed sources at the connection nodes of the segments will result in a tedious work. Shinh *et al*. presented a SPICE macro-model for transient analysis of lossy MTLs in the presence of incident electromagnetic fields [13]. However, the model is solved in the mode-domain, as for the nonlinear problems, a phase-domain model is preferred. In [14], a SPICE compatible multiport model for MTLs excited by an incident electromagnetic field is proposed, but it cannot be applied to analyze the lossy transmission lines [14]. As for the calculation of LIOVs of MTLs, Lightning Induced Voltage (LIV) is a popular circuit solver compatible method, which has been integrated into ATP software through the ''MODELS'' language [15], [16]. Another computer code developed by an international collaboration leading by Rachidi and Nucci, named as LIOV code [17], has been widely used to analyze the LIOVs of distributed networks. The early version of the LIOV code was interfaced with the EMTP 96, whereas a more recent version has been interfaced with the EMTP-RV [18]. Recently, a model and numerical solution using the PSCAD platform are proposed, in which the coupling equations are written in Fortran and embedded into the power system model to communicate with the boundaries and the discontinuity points of the MTLs. In [19] and [20], a method belonging to the analytical category, named as Circuit Lightning-Induced Voltage (CiLIV), is proposed by Maffucci and Miano [21] and is integrated into SimPowerSystems in MATLAB, in which the transmission line model is described by its characteristic admittance and treated by the method in. In [22], a DEPACT-LIOVs macro-model is proposed and integrated into PSCAD in order to improve the efficiency. However, this method is not strict in theory because it is based on an assumption that the incident electric fields only couple with the lossless sections of the transmission lines. Moreover, the synthesis method used to model the frequency dependent networks may result in a passivity violation problem, i.e., some negative value circuit elements may appear in the resultant circuit.

The aim of this paper is to develop a circuit model which can be directly integrated into the circuit simulators with the built-in models/setups. Firstly, an macro-model of the Agrawal's field-to-line coupling model is derived, in which the distributed equivalent voltage sources due to the horizontal components of the incident electric fields are lumped at the terminals of the transmission lines. In order to interface with MATLAB/Simulink, the propagation function $\boldsymbol{H}$ is approximated by the vector fitting (VF) method [23], and then described by a state-space representation [24]. The MTLs are modeled as a passive equivalent circuit by means of the Brune's synthesis [25], which can overcome the passivity violation problem. Furthermore, considering that the peak values of the LIOVs are mainly concerned in the insulation coordination, a more simple model for evaluation of the early time response is proposed, and the procedure of calculating LIOVs can be further simplified.

This paper is organized as follows. In Section II, a macro-model for evaluating the Agrawal's field-to-line coupling model is derived in detail, and a more simple model used for evaluating the early time response of LIOVs is proposed in Section III. In Section IV, some numerical examples are provided to show the accuracy of the proposed method, and the influence of the metal oxide arrester (MOA) and ground wire on LIOVs are discussed. In Section V, some conclusions are presented.

II. MACRO-MODEL FOR FIELD-TO-LINE COUPLING MODEL

Agrawal's filed-to-line coupling model is one of the simple and accurate models for calculating LIOVs. The modified telegrapher's equation of the lossy MTLs illuminated by the external fields can be written as

$$\begin{cases} \dfrac{d\boldsymbol{U}^s(x)}{dx} + \left[s\boldsymbol{L}_0 + \boldsymbol{R}_0 + \boldsymbol{Z}_g(s)\right] \cdot \boldsymbol{I}(x) = \boldsymbol{E}_x(x) \\ \dfrac{d\boldsymbol{I}(x)}{dx} + (s\boldsymbol{C}_0 + \boldsymbol{G}_0) \cdot \boldsymbol{U}(x) = \boldsymbol{0}, \end{cases} \tag{1}$$

where $\boldsymbol{U}^s(x)$ and $\boldsymbol{I}(x)$ are the scatter voltage and total current vector at location x in the complex frequency domain, respectively. $\boldsymbol{R}_0$, $\boldsymbol{G}_0$, $\boldsymbol{L}_0$ and $\boldsymbol{C}_0$ are the resistance, conductance, inductance, and capacitance matrices per-unit-length (p.u.l.), $\boldsymbol{E}_x(s)$ is the horizontal incident electric field along the line, and $\boldsymbol{Z}_g(s)$ is the frequency dependent impedance p.u.l. corresponding to the skin effect of the conductor and the lossy ground [26].

The total voltage $\boldsymbol{U}(x)$ is given by

$$\boldsymbol{U}(x) = \boldsymbol{U}^s(x) + \boldsymbol{U}_z(x), \tag{2}$$

where $\boldsymbol{U}_z(x)$ is the voltage due to the vertical component of the incident electric field $\boldsymbol{E}_z(x, z)$, and it is can be evaluated by

$$\boldsymbol{U}_z(x) = -\int_0^h E_z(x, z)\, dz. \tag{3}$$

In order to solve (1), the phasor quantities can be converted into their mode counterparts by a similarity transformation [4], i.e.,

$$\begin{cases} \boldsymbol{U}^s(x) = \boldsymbol{T}_v \boldsymbol{U}_m^s(x) \\ \boldsymbol{I}(x) = \boldsymbol{T}_i \boldsymbol{I}_m(x), \end{cases} \tag{4}$$

where $\boldsymbol{T}_v$ and $\boldsymbol{T}_i$ are the similarity transformation matrices according to the voltage and current vector, respectively.

Substituting (4) into (1) yields

$$\begin{cases} \dfrac{d\boldsymbol{U}_m^s}{dx} + \boldsymbol{Z}_{0m} \cdot \boldsymbol{I}_m(x) = \boldsymbol{T}_v^{-1} \boldsymbol{E}_x(x) \\ \dfrac{d\boldsymbol{I}_m}{dx} + \boldsymbol{Y}_{0m} \cdot \boldsymbol{U}_m^s(x) = \boldsymbol{0}, \end{cases} \tag{5}$$

where $\boldsymbol{Z}_{0m} = \boldsymbol{T}_v^{-1}\left[s\boldsymbol{L}_0 + \boldsymbol{R}_0 + \boldsymbol{Z}_g(s)\right] \cdot \boldsymbol{T}_i$ and $\boldsymbol{Y}_{0m} = \boldsymbol{T}_i^{-1}(s\boldsymbol{C}_0 + \boldsymbol{G}_0) \cdot \boldsymbol{T}_v$, respectively. The analytical solution to (5) can be written as

$$\begin{cases} \boldsymbol{I}_m(x_1) = \boldsymbol{Y}_{Cm}\boldsymbol{U}_m^s(x_1) - e^{-\boldsymbol{\gamma}_m(x_2-x_1)}\left[\boldsymbol{I}_m(x_2) + \boldsymbol{Y}_{Cm}\boldsymbol{U}_m^s(x_2)\right] \\ \qquad + \boldsymbol{Y}_{Cm}\int_{x_1}^{x_2} e^{-\boldsymbol{\gamma}_m(x'-x_1)} \cdot \left[\boldsymbol{T}_v^{-1} \cdot \boldsymbol{E}_x\left(x'\right)\right] dx' \\ \boldsymbol{I}_m(x_2) = \boldsymbol{Y}_{Cm}\boldsymbol{U}_m^s(x_2) - e^{-\boldsymbol{\gamma}_m(x_2-x_1)}\left[\boldsymbol{I}_m(x_1) + \boldsymbol{Y}_{Cm}\boldsymbol{U}_m^s(x_1)\right] \\ \qquad - \boldsymbol{Y}_{Cm}\int_{x_1}^{x_2} e^{-\boldsymbol{\gamma}_m(x_2-x')} \cdot \left[\boldsymbol{T}_v^{-1} \cdot \boldsymbol{E}_x\left(x'\right)\right] dx'. \end{cases} \tag{6}$$

where $\boldsymbol{Y}_{Cm}$ and γ_m are the mode characteristic admittance matrix and mode propagation constant, respectively. x_1 and x_2 are the locations of the near and far end of the lines, respectively. Substituting the inverse transformation of (4) into (6), the solution to (1) can be obtained and given by

$$\begin{cases} \boldsymbol{I}(x_1) = \boldsymbol{Y}_C \cdot \boldsymbol{U}^s(x_1) - \boldsymbol{H}(x_2-x_1) \cdot \left[\boldsymbol{I}(x_2) + \boldsymbol{Y}_C \cdot \boldsymbol{U}^s(x_2)\right] \\ \qquad + \boldsymbol{Y}_C \cdot \int_{x_1}^{x_2} \boldsymbol{H}^T\left(x'-x_1\right) \cdot \boldsymbol{E}_x\left(x'\right) dx' \\ \boldsymbol{I}(x_2) = \boldsymbol{Y}_C \cdot \boldsymbol{U}^s(x_2) - \boldsymbol{H}(x_2-x_1) \cdot \left[\boldsymbol{I}(x_1) + \boldsymbol{Y}_C \cdot \boldsymbol{U}^s(x_1)\right] \\ \qquad - \boldsymbol{Y}_C \cdot \int_{x_1}^{x_2} \boldsymbol{H}^T\left(x_2-x'\right) \cdot \boldsymbol{E}_x\left(x'\right) dx', \end{cases} \tag{7}$$

where $\boldsymbol{Y}_C = \boldsymbol{T}_i\boldsymbol{Y}_{Cm}\boldsymbol{T}_v^{-1}$ is known as the characteristic admittance matrix of MTLs, and $\boldsymbol{H}(x) = e^{-\boldsymbol{\gamma}x}$ are called the propagation functions, in which the propagation constant can be evaluated by $\boldsymbol{\gamma} = \sqrt{\boldsymbol{Y}_0\boldsymbol{Z}_0}$, and $\boldsymbol{Y}_0$ and $\boldsymbol{Z}_0$ are the shunt admittance and series impedance matrices p.u.l. of MTLs, respectively.

By defining two categories of current source, i.e.,

$$\begin{cases} \boldsymbol{I}_s(x_1) = -\boldsymbol{H}(x_2-x_1) \cdot \left[\boldsymbol{I}(x_2) + \boldsymbol{Y}_C \cdot \boldsymbol{U}^s(x_2)\right] \\ \boldsymbol{I}_s(x_2) = -\boldsymbol{H}(x_2-x_1) \cdot \left[\boldsymbol{I}(x_1) + \boldsymbol{Y}_C \cdot \boldsymbol{U}^s(x_1)\right], \end{cases} \tag{8}$$

which are related to the reflections from the other end and

$$\begin{cases} \boldsymbol{I}_E(x_1) = \boldsymbol{Y}_C \cdot \int_{x_1}^{x_2} \boldsymbol{H}^T\left(x'-x_1\right) \cdot \boldsymbol{E}_x\left(x'\right) dx' \\ \boldsymbol{I}_E(x_2) = -\boldsymbol{Y}_C \cdot \int_{x_1}^{x_2} \boldsymbol{H}^T\left(x_2-x'\right) \cdot \boldsymbol{E}_x\left(x'\right) dx', \end{cases} \tag{9}$$

which are determined by the external fields, equation (7) can be rewritten as

$$\begin{cases} \boldsymbol{I}(x_1) = \boldsymbol{Y}_C \cdot \boldsymbol{U}^s(x_1) + \boldsymbol{I}_s(x_1) + \boldsymbol{I}_E(x_1) \\ \boldsymbol{I}(x_2) = \boldsymbol{Y}_C \cdot \boldsymbol{U}^s(x_2) + \boldsymbol{I}_s(x_2) + \boldsymbol{I}_E(x_2). \end{cases} \tag{10}$$

III. EQUIVALENT CIRCUIT FOR EVALUATION OF LIOVS IN MATLAB/SIMULINK

Without loss of generality, in this section, a three-conductor transmission lines system is adopted to interpret the modeling procedure. According to (10), a multiport equivalent circuit can be modeled and shown in Fig. 1.

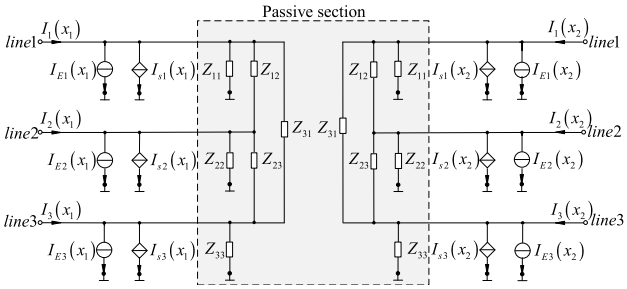

FIGURE 1. Equivalent circuit of the Agrawal's field-to-line coupling model. (three-conductor transmission lines system).

A. EQUIVALENT CIRCUIT OF THE PASSIVE SECTION

The passive section in Fig. 1 can be described by the characteristic admittance matrix $\boldsymbol{Y}_C$, which is

$$\boldsymbol{Y}_C = \begin{bmatrix} Y_{C,11} & Y_{C,12} & Y_{C,13} \\ Y_{C,21} & Y_{C,22} & Y_{C,23} \\ Y_{C,31} & Y_{C,32} & Y_{C,33} \end{bmatrix} \quad \left(Y_{C,ij} = Y_{C,ji}, i \neq j\right), \tag{11}$$

in which all the elements are frequency dependent because of the consideration of the skin effect and ground return impedance. From a circuit theory perspective, the impedance $\boldsymbol{Z}_{ii}$ between node i and ground reference and $\boldsymbol{Z}_{ij}$ between node i and j can be evaluated by

$$Z_{ij}(s) = \begin{cases} 1/\sum_{j=1}^{3} Y_{C,ij} & i = j \\ -1/Y_{C,ij} & i \neq j \end{cases} \tag{12}$$

Taking advantage of the VF, Z_{ij} can be approximated by

$$Z_{ij}(s) = R_{dij} + \sum_{k=1}^{N_r} Z_k(s) + \sum_{m=1}^{N_m} Z_m(s), \tag{13}$$

where $R_{dij} = \lim_{s\to\infty} Z(s)$, and

$$\begin{cases} Z_k(s) = \dfrac{r_k}{s - p_k} \\ Z_m(s) = \left(\dfrac{r_m}{s - p_m} + \dfrac{r_m^*}{s - p_m^*}\right), \end{cases} \tag{14}$$

in which r_k, p_k, r_m and $p_m$are the real residue, real pole, complex residue and complex pole, respectively. r_m^* and p_m^* are the complex conjugates of r_m and p_m. It is well known that the network shown in Fig. 2 is a simple way to achieve the equivalent circuit of $\boldsymbol{Z}_{ij}$.

As for the sub-item impedance $Z_k(s)$ in Fig. 2, the values of R_k and C_k can be evaluated by

$$R_k = -\frac{r_k}{p_k}, \quad C_k = \frac{1}{r_k}, \tag{15}$$

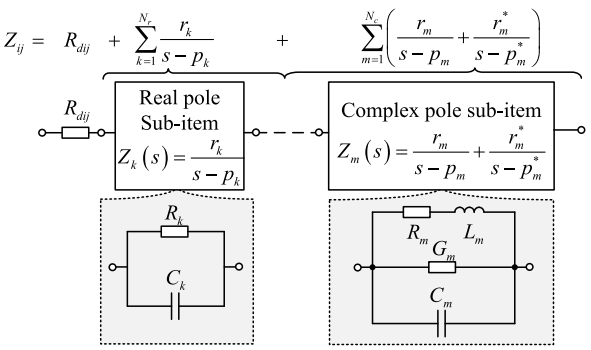

FIGURE 2. Equivalent circuit of Z_{ij}.

and the values of the circuit elements corresponding to $Z_m(s)$ with complex residues and poles are

$$\begin{cases} C_m = \dfrac{1}{r_m + r_m^*} \\ G_m = \dfrac{1}{r_m + r_m^*}\left[-\left(p_m + p_m^*\right) + \dfrac{r_m p_m^* + r_m^* p_m}{r_m + r_m^*}\right] \\ L_m = \dfrac{r_m + r_m^*}{p_1 p_2 + \frac{r_m p_m^* + r_m^* p_m}{r_m + r_m^*}\left[-\left(p_m + p_m^*\right) + \frac{r_m p_m^* + r_m^* p_m}{r_m + r_m^*}\right]} \\ R_m = \dfrac{-\left(r_m p_m^* + r_m^* p_m\right)}{p_1 p_2 + \frac{r_m p_m^* + r_m^* p_m}{r_m + r_m^*}\left[-\left(p_m + p_m^*\right) + \frac{r_m p_m^* + r_m^* p_m}{r_m + r_m^*}\right]}. \end{cases} \tag{16}$$

From a circuit theory viewpoint, the following necessary condition must be satisfied in order to achieve a passive circuit [27]

$$r_k \geq 0 \text{ and } \begin{cases} r_m p_m^* + r_m^* p_m \leq 0 \\ r_m p_m - r_m^* p_m^* \leq 0, \end{cases} \tag{17}$$

i.e., the values of all the circuit elements of $Z_k(s)$ and $Z_m(s)$ must be positive. Sometimes, this condition may not be satisfied and a passivity violation problem would be introduced although the ''macro passivity'' can be guaranteed by VF. The reason is that VF is a mathematical approximation method which cannot guarantee the ''micro passivity'' of every sub-item. In order to address this problem, Brune's synthesis is adopted to build the equivalent circuit of Z_{ij} because it can be bound to achieve a passive circuit. A detailed Brune's realization can be found in [28], in which a four-step extraction procedure, also known as ''Brune cycle'', is involved and the passivity of each sub-circuit can be ensured. By means of Brune's synthesis, an equivalent circuit according to the passive section in Fig. 1 can be achieved and it can be built in MATLAB/Simulink with its built-in *R*/*L*/*C* components. For the rationality of the article arrangement, example 1 given in Section V is presented here. All impedances in Fig. 1 are approximated by (13) with $N_r = 6$ and $N_m = 0$, and the values of R_{dij}, $r_{ij,k}$ and $p_{ij,k}$ are listed in Table 3 in the appendix. A. Taking Z_{11} and Z_{12} as examples, their equivalent circuits are given in Fig. 13 and Fig. 14, respectively, which are also provided in the appendix. A. Accordingly, the amplitude-frequency and phase-frequency characteristics are shown in Fig. 15 and Fig. 16, which validates the equivalent circuits.

B. REALIZATION OF I_s (x_1) AND I_s (x_2) IN MATLAB/SIMULINK

In order to obtain an accurate time domain description of the propagation function $\boldsymbol{H}$, it is necessary to extract some time-delay items [29] first. Taking advantage of the similarity transformation, $\boldsymbol{H}$ can be expressed by [30]

$$\boldsymbol{H} = \boldsymbol{T}_i \boldsymbol{H}_m \boldsymbol{T}_i^{-1}, \tag{18}$$

where $\boldsymbol{H}_m$ is the mode-domain propagation function, given by

$$\boldsymbol{H}_m = diag\left[e^{-\gamma_{m1} l}, e^{-\gamma_{m2} l}, e^{-\gamma_{m3} l}\right], \tag{19}$$

where l is the length of the line. By partitioning $\boldsymbol{T}_i$ in columns and $\boldsymbol{T}_i^{-1}$ in rows, $\boldsymbol{H}$ can be rewritten as [31]

$$\boldsymbol{H} = \sum_{i=1}^{3} \boldsymbol{D}_i e^{-\bar{\gamma}_{mi} l} e^{-s\tau_i}, \tag{20}$$

where $\boldsymbol{D}_i$ is the product of the ith column of $\boldsymbol{T}_i$ and the ith row of $\boldsymbol{T}_i^{-1}$, and $e^{-\bar{\gamma}_{mi} l}$ is a minimum-phase-shift (mps) function. τ_i is the time delay associated with the ith mode velocity, which can be evaluated by [29]

$$\tau_i = \frac{l}{v_i(\omega)} + \frac{\varphi_{mps}(\omega)}{\omega}, \tag{21}$$

where $v_i(\omega)$ is the velocity of the ith mode. $\varphi_{mps}(\omega)$ denotes the mps angle of the magnitude function $|\boldsymbol{H}(\omega)|$, which can be calculated by the method proposed in [29].

By means of VF, $\boldsymbol{H}$ can be approximated by

$$\boldsymbol{H} = \sum_{i=1}^{3} \boldsymbol{H}_i = \sum_{i=1}^{3} e^{-s\tau_i} \sum_{k=1}^{N_h} \frac{\boldsymbol{Q}_{k,i}}{s - \bar{p}_{k,i}}, \tag{22}$$

where $\boldsymbol{Q}_{k,i}$ is the kth residue matrix of $\boldsymbol{H}$ corresponding to the kth pole related to the ith mode, and N_h is the fitting order.

In order to interface with MATLAB/Simulink, the state-space representation of $\boldsymbol{I}_s(x_1)$ and $\boldsymbol{I}_s(x_2)$ are established. Taking $\boldsymbol{I}_s(x_1)$ as an example, the first equation in (8) can be rewritten as

$$\boldsymbol{I}_s(x_1) = -\sum_{i=1}^{3} \boldsymbol{I}_{s,i}(x_1), \tag{23}$$

and each element $\boldsymbol{I}_{s,i}(x_1)$ can be evaluated by

$$\boldsymbol{I}_{s,i}(x_1) = \sum_{k=1}^{N_h} \frac{\boldsymbol{Q}_{k,i}}{s - \bar{p}_{k,i}} \cdot e^{-s\tau_i} \cdot \boldsymbol{I}_{ref}(x_1), \tag{24}$$

where $\boldsymbol{I}_{ref}(x_1) = \boldsymbol{I}(x_2) + \boldsymbol{Y}_C \cdot \boldsymbol{U}^s(x_2)$. By means of the inverse Laplace transformation, (24) can be expressed by the following state-space representation with retardation, i.e.,

$$\begin{cases} \dfrac{d}{dt}\boldsymbol{x} = \boldsymbol{A}\boldsymbol{x} + \boldsymbol{B} \cdot \boldsymbol{i}_{ref}(t - \tau_i) \\ \boldsymbol{i}_{s,i}(x_1, t) = \boldsymbol{C}\boldsymbol{x} + \boldsymbol{D} \cdot \boldsymbol{i}_{ref}(t - \tau_i), \end{cases} \tag{25}$$

where $\boldsymbol{x} = \left[\boldsymbol{i}_{s,1,i} \cdots \boldsymbol{i}_{s,N_h,i}\right]^T$, and the coefficient matrices are $\boldsymbol{A} = \begin{bmatrix} \bar{\boldsymbol{p}}_{1,i} & & \\ & \ddots & \\ & & \bar{\boldsymbol{p}}_{N_h,i} \end{bmatrix}$, $\boldsymbol{B} = \begin{bmatrix} \boldsymbol{Q}_{1,i} \\ \vdots \\ \boldsymbol{Q}_{N_h,i} \end{bmatrix}$, $\boldsymbol{C} = \left[\boldsymbol{1} \cdots \boldsymbol{1}\right]$, and $\boldsymbol{D}$=$\boldsymbol{0}$. The kth element of matrix $\boldsymbol{A}$ is $\bar{\boldsymbol{p}}_{k,i} = \begin{bmatrix} \bar{p}_{k,i} & & \\ & \bar{p}_{k,i} & \\ & & \bar{p}_{k,i} \end{bmatrix}$, and the matrix $\boldsymbol{1}$ in $\boldsymbol{C}$ is a 3×3 identity matrix. The above state-space representation can be implemented by using the "State-Space" component in MATLAB/Simulink, whose parameters can be set as $\boldsymbol{A}$, $\boldsymbol{B}$, $\boldsymbol{C}$, and $\boldsymbol{D}$, and $\boldsymbol{i}_s(x_1, t)$ can be obtained by

$$\boldsymbol{i}_s\left(x_1, t\right) = -\sum_{i=1}^{3} \boldsymbol{i}_{s,i}\left(x_1, t\right), \tag{26}$$

In a similar way, the current source $\boldsymbol{i}_s(x_2, t)$ can also be evaluated.

C. EVALUATION OF $I_E(x_1)$ AND $I_E(x_2)$

Equation (9) can be rewritten as

$$\begin{cases} \boldsymbol{I}_E\left(x_1\right) = \boldsymbol{Y}_C \cdot \boldsymbol{U}_E\left(x_1\right) \\ \boldsymbol{I}_E\left(x_2\right) = -\boldsymbol{Y}_C \cdot \boldsymbol{U}_E\left(x_2\right), \end{cases} \tag{27}$$

where

$$\begin{cases} \boldsymbol{U}_E\left(x_1\right) = \displaystyle\int_{x_1}^{x_2} \boldsymbol{H}^T\left(x' - x_1\right) \cdot \boldsymbol{E}_x\left(x'\right) dx' \\ \boldsymbol{U}_E\left(x_2\right) = \displaystyle\int_{x_1}^{x_2} \boldsymbol{H}^T\left(x_2 - x'\right) \cdot \boldsymbol{E}_x\left(x'\right) dx'. \end{cases} \tag{28}$$

Using VF to approximate all the elements of $\boldsymbol{Y}_C$ with a common set of poles, i.e., $\{p_1, p_2, \ldots\ldots, p_{Ny}\}$. Taking $\boldsymbol{I}_E(x_1)$ as an example, it can be expressed as (29), and its time domain counterpart can be expressed as (30) by means of the inverse Laplace transformation and Eulerian backward difference.

$$\boldsymbol{i}_E\left(x_1, t_n\right) = \sum_{k=1}^{N_y} \boldsymbol{i}_{E,k}\left(x_1, t_n\right), \tag{29}$$

where N_y is fitting order of $\boldsymbol{Y}_C$, and

$$\begin{aligned} \boldsymbol{i}_{E,k}(x_1, t_n) = {} & c_k \boldsymbol{i}_{E,k}(x_1, t_{n-1}) \\ & + \boldsymbol{d}_k\left[\boldsymbol{u}_E(x_1, t_n) + \boldsymbol{u}_E(x_1, t_{n-1})\right], \end{aligned} \tag{30}$$

where

$$\begin{cases} c_k = \left[(2 + \Delta t \cdot p_k)/(2 - \Delta t \cdot p_k)\right] \\ \boldsymbol{d}_k = (\Delta t \cdot \boldsymbol{R}_k)/(2 - \Delta t \cdot p_k), \end{cases}$$

in which $\boldsymbol{R}_k$ is the kth residue matrix of $\boldsymbol{Y}_C$ corresponding to the kth pole p_k and Δt is the step size.

As for the evaluation of $\boldsymbol{u}_E(x_1, t_n)$ in (30), the following procedures are implemented. Firstly, a rectangular integration is adopted to evaluate (28) by dividing the line into N_x segments corresponding to the number of $\boldsymbol{E}_x$, given by

$$\begin{cases} \boldsymbol{U}_E\left(x_1\right) = \displaystyle\sum_{m=1}^{N_x} \boldsymbol{H}^T\left(x_m - x_1\right) \cdot \boldsymbol{E}_x\left(x_m\right) \Delta x \\ \boldsymbol{U}_E\left(x_2\right) = \displaystyle\sum_{m=1}^{N_x} \boldsymbol{H}^T\left(x_2 - x_m\right) \cdot \boldsymbol{E}_x\left(x_m\right) \Delta x, \end{cases} \tag{31}$$

where $\Delta x = (x_2 - x_1)/N_x$. For example, as for a 1km-long line, it can be equally discretized into 100 segments, i.e., the length of each segment is 10m. Secondly, in a similar way to (22), the propagation function $\boldsymbol{H}^T(x_m - x_1)$ in (31) can be expressed as (32),

$$\boldsymbol{H}^T\left(x_m - x_1\right) = \sum_{i=1}^{3} e^{-s\tau_{m,i}} \sum_{k=1}^{N_h} \frac{\boldsymbol{Q}_{m,k,i}^T}{s - \hat{p}_{m,k,i}}, \tag{32}$$

where $\tau_{m,i}$ is the time delay related to the distance from x_1 to x_m, and $\boldsymbol{Q}_{m,k,i}^T$ is the residue matrix of $\boldsymbol{H}^T(x_m - x_1)$ corresponding to the kth pole $\hat{p}_{m,k,i}$ related to the ith mode. Finally, substituting (32) into the first formula in (31) and taking advantage of inverse Laplace transformation, (31) can be expressed in the time domain, given by

$$\boldsymbol{u}_E\left(x_1, t_n\right) = \sum_{m=1}^{N_x} \sum_{i=1}^{3} \sum_{k=1}^{N_h} \boldsymbol{u}_{E,m,k,i}\left(x_1, t_n\right), \tag{33}$$

where

$$\begin{aligned} \boldsymbol{u}_{E,m,k,i}\left(x_1, t_n\right) = {} & a_{m,k,i} \boldsymbol{u}_{E,m,k,i}\left(x_1, t_{n-1}\right) \\ & + \boldsymbol{b}_{m,k,i}\left[\boldsymbol{E}_{x,m}\left(x_i, t_n - \tau_{m,i}\right)\right. \\ & \left. + \boldsymbol{E}_{x,m}\left(x_i, t_{n-1} - \tau_{m,i}\right)\right] \Delta x, \end{aligned} \tag{34}$$

in which

$$\begin{cases} a_{m,k,i} = \left(2 + \Delta t \cdot \hat{p}_{m,k,i}\right)/\left(2 - \Delta t \cdot \hat{p}_{m,k,i}\right) \\ \boldsymbol{b}_{m,k,i} = \left(\Delta t \cdot \boldsymbol{Q}_{m,k,i}^T\right)/\left(2 - \Delta t \cdot \hat{p}_{m,k,i}\right). \end{cases}$$

As for the current $\boldsymbol{i}_E(x_2, t)$ at the other end, it can be evaluated in a similar way. Considering that $\boldsymbol{i}_E(x_1, t)$ and $\boldsymbol{i}_E(x_2, t)$ are only determined by the external fields, they can be precalculated first and then imported into MATLAB/Simulink as current generators for the evaluation of LIOVs.

IV. SIMPLIFIED MODEL FOR EVALUATION OF THE EARLY TIME RESPONSE OF LIOVS

Considering that the peak values of the LIOVs are mainly concerned in the insulation coordination, in this section, a more simple model for the early time response is proposed, which can be used to evaluate the peak values of LIOVs.

It is well known that the time delay depends on the length of lines l and propagation velocity v. As long as the time delay from one end to the other is longer than the rising time of LIOVs, the peaks of LIOVs would not be dependent of the current sources $\boldsymbol{I}_s(x_1)$ and $\boldsymbol{I}_s(x_2)$. So it can be concluded that one could accurately evaluate the peak values of LIOVs with a simplified circuit shown in Fig. 3, named as "early time model" in this paper.

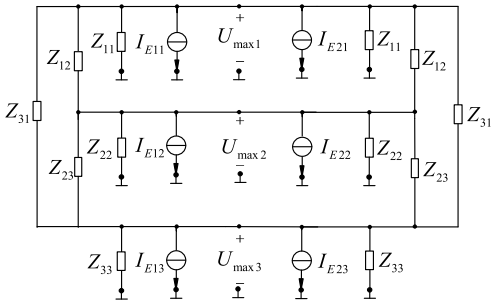

FIGURE 3. The "early time model" for evaluation of the peak of LIOVs (three conductor transmission lines).

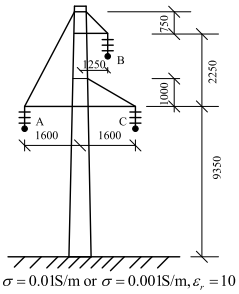

FIGURE 4. A 35kV three-phase overhead line configuration.

Compared Fig. 3 with Fig. 1, the "early time model" is more simple, which is suitable for the insulation coordination of the distributed networks. The accuracy of the "early time model" will be illustrated by a comparison with the "exact model" in Section V. Furthermore, the variation of the rising time of LIOVs with the length of line is shown in the appendix. B, which indicates how to achieve the effective length of the line in the "early time model".

V. SIMULATION AND DISCUSSION

In this section, three examples are provided to demonstrate the accuracy of the proposed model. As for the description of the lightning return stroke, Heidler's functions are adopted to describe the channel base current [32]. The peak value of the channel base current is adopted as 35kA and its maximum time-derivative is 120kA/μs. The lightning current is allowed to decrease with the height while propagating the channel upward, and the current along the channel can be expressed by

$$\begin{cases} i\left(z',t\right) = i\left(0, \dfrac{t-z'}{v_c}\right)\exp\left(\dfrac{-z'}{\lambda}\right) & \dfrac{t \geq z'}{v_c} \\ i\left(z',t\right) = 0 & \dfrac{t \leq z'}{v_c}, \end{cases} \tag{35}$$

where v_c is the return stroke velocity and is assumed to be 1.3×10^8m/s, λ is the decay constant which takes into account the effect of the vertical distribution of charge stored in the corona sheath of the leader, and subsequently, discharge during the return stroke phase, and its value has been assumed to be 2km [33].

A. EXAMPLE 1

In this example, a 1km-long three-phase transmission lines system is studied. The conductors are placed at different heights, as shown in Fig. 4. Each conductor is terminated with a resistance which equals to its characteristic impedance determined in the absence of the other conductors.

The striking point is considered equidistant from the line terminations and a distance of 50m from the pole, and the lightning electromagnetic fields are calculated by the method in [34]–[37]. In this paper, the radial electric fields of the observation points far from the lightning striking point (larger than 100m) over the homogenous lossy ground can be calculated by the Cooray–Rubinstein formula [34], [35], while the numerical Sommerfeld integral with an improved complex integration path [36] or the FDTD method [37] is used for the observation points located at very closed to the lightning striking point (smaller than 100m) over the homogenous or two layer stratified lossy ground. The LIOVs of the conductors above a lossy ground with different ground conductivities (0.01S/m and 0.001S/m) are calculated. The voltages of the terminal and the middle point of phase B are shown in Fig. 5, while the corresponding results in [3] are given in the same figure. As can be seen, within the validity limits, the proposed model provides solutions in good agreement with TDFEM.

A comparison between the "early time model" and exact mode is carried out, and the corresponding calculated results are shown in Fig. 6. As can be seen, the early time period transients voltages are in good agreement which indicates that the "early time model" can accurately evaluate the peak value of LIOVs in a simple way.

B. EXAMPLE 2

In this example, the effect of ground wire on the lightning-induced voltages of overhead transmission lines is discussed. The configuration of an overhead lines system with a ground wire placed on the top of the pole is shown in Fig. 7, and there are nine poles along the 1km-long line, i.e., the distance between each pole is 100m. The grounding resistance R_g and the equivalent inductance of the pole L_g are adopted as 15Ω and 12.6μH, respectively. The corresponding equivalent circuit is shown in Fig. 8, in which the sub-unit of the equivalent circuit is same as Fig. 1. Each conductor is terminated with a resistance equal to its characteristic impedance determined in the absence of the other conductors.

The induced voltages of phase C and the ground wire are shown in Fig. 9 while the corresponding results calculated by TDFEM are given in the same figure. As can be seen, within an acceptable tolerance, the proposed model provides solutions in good agreement with TDFEM.

Fig. 10 shows the LIOVs at the midpoint of the three phase conductors and the ground wire, and the peaks of the LIOVs with and without ground wire are listed in Table 1. As can be seen, the presence of the ground wire can reduce the LIOVs to some extent because of the shielding effect due to the presence of the ground wire.

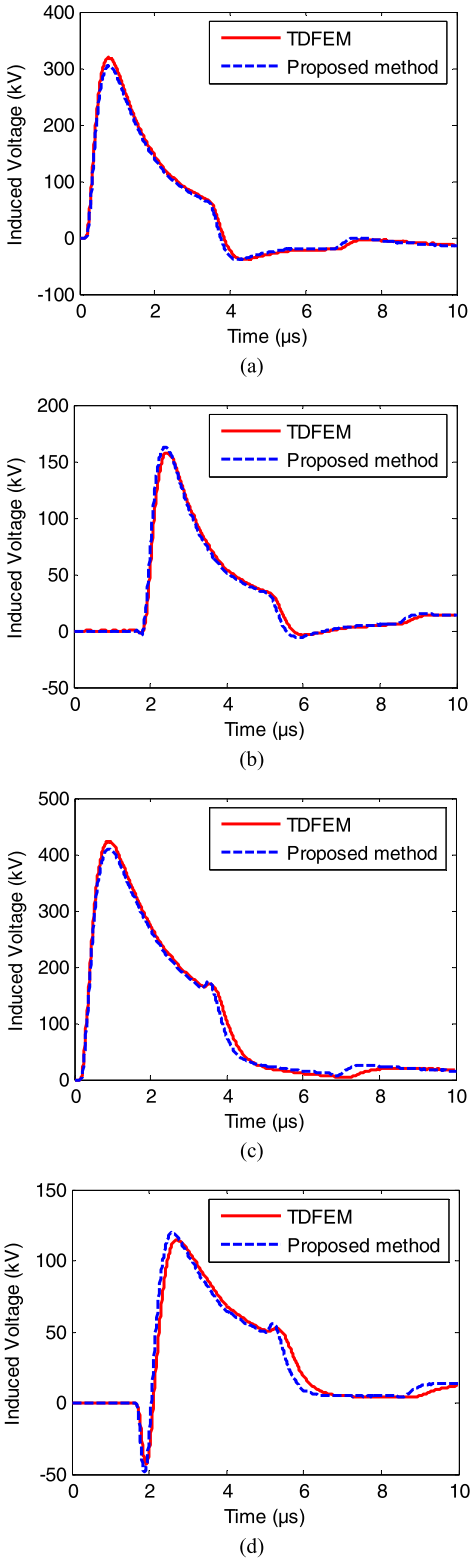

FIGURE 5. Lightning induced voltages at different positions of phase B. (a) middle point ($\sigma = 0.01$S/m), (b) termination ($\sigma = 0.01$S/m). (c) middle point ($\sigma = 0.001$S/m), (d) termination ($\sigma = 0.001$S/m).

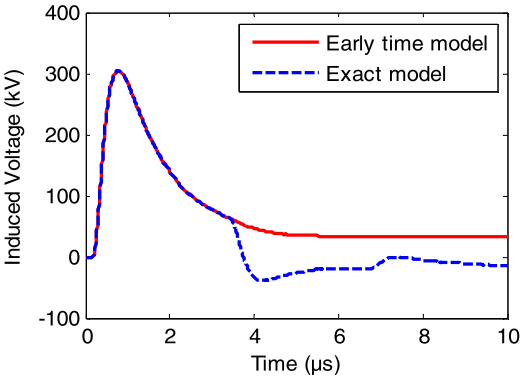

FIGURE 6. Comparison of the lightning induced voltages at the middle of phase B between exact model and early time model ($\sigma = 0.01$S/m).

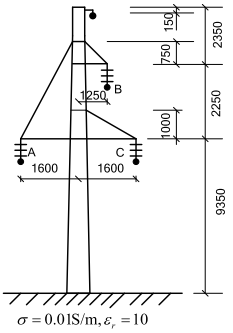

FIGURE 7. A 35kV three-phase overhead line configuration with ground wire.

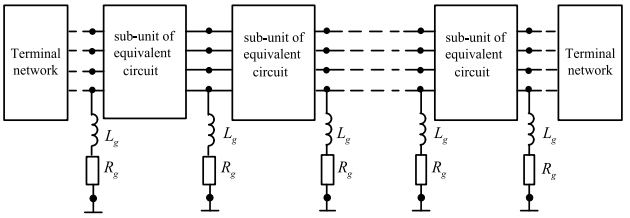

FIGURE 8. Equivalent circuit with ground wire.

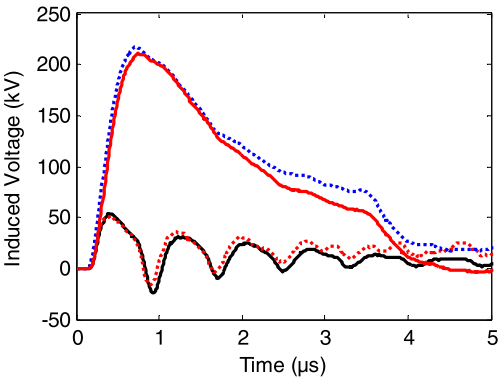

FIGURE 9. Comparison of voltage induced on phase C and ground wire between the macro model(dot lines) and TDFEM(solid lines).

C. EXAMPLE 3

Metal oxide arrester (MOA) has been widely used to reduce the damage of the overhead transmission lines caused by lightning. In this example, the influence of MOA on LIOVs is investigated. The parameters of the overhead lines are the same as the configuration shown in Fig. 4 and a MOA is

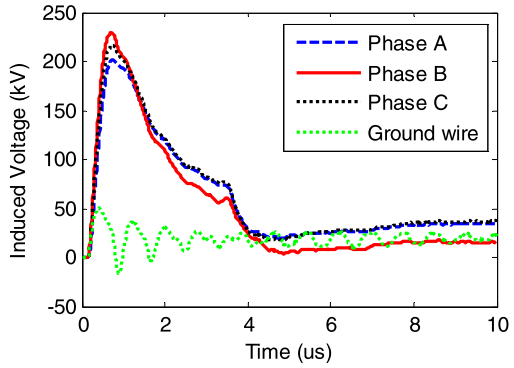

FIGURE 10. Induced overvoltages on the three-line conductors with ground wire.

TABLE 1. Peak values of LIOVs with and without ground wire.

Phase	without ground wire(kV)	with ground wire(kV)	Reduction Ratio
A	254.2	202.2	20.5%
B	308.5	230.1	25.4%
C	266.1	217.2	18.4%

equipped on phase A in the middle point of the 1-km long line. MOA exhibits an extremely high resistance during normal operation and a very low resistance during transient overvoltages [3]. In this paper, the MOA is considered as an nonlinear resistor whose V-I characteristic can be represented by

$$u = \begin{cases} 146.46 \times 10^3 \cdot i^{0.2} & 0\text{mA} \le i < 1\text{mA} \\ 51.97 \times 10^3 \cdot i^{0.05} & 1\text{mA} \le i < 1\text{A} \\ 51.97 \times 10^3 \cdot i^{0.06} & 1\text{A} \le i < 6\text{kA}. \end{cases} \quad (36)$$

The nonlinear resistor can be implemented by the "Surge Arrester" component in MATLAB/Simulink. The nonlinear V-I characteristic of the surge arrester is described by a series of exponential functions, i.e.,

$$u = \left(k_m u_{ref} / \left(i_{ref}\right)^{1/\alpha_m}\right) i^{1/\alpha_m}, \quad (37)$$

where i_{ref} is the reference current (usually 500 A or 1 kA), and u_{ref} is the protection voltage according to the reference current. k_m and α_m are the coefficients used to describe the mth section of the V-I characteristic curve, and $m = 1, 2, 3$ are related to the small current, the nonlinear and the saturation region, respectively.

Compared with (36), the relevant parameters k_m and α_m in (37) can be easily obtained, which are listed in Table 2. The V-I characteristic curve of the nonlinear resistance in MATLAB/Simulink is shown in Fig. 11, while the corresponding curve described by (36) is also given in the same figure, as can be seen, they are in good agreements.

The LIOVs are evaluated and shown in Fig. 12. As can be seen, the placement of MOA can limit the voltage of the phase A effectively. Moreover, the voltages of other phases can also be reduced in some degree due to the coupling mechanism between the conductors.

TABLE 2. Related parameters of "Surge Arrester" in MATLAB/Simulink.

	i_{ref}			u_{ref}	
	1000A			78660V	
k_1	k_2	k_3	α_1	α_2	α_3
7.41	0.933	1	5	20	16.67

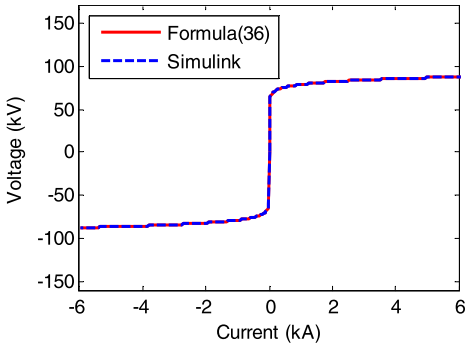

FIGURE 11. V-I characteristic of formula (36) and "Surge Arrester" in MATLAB/Simulink.

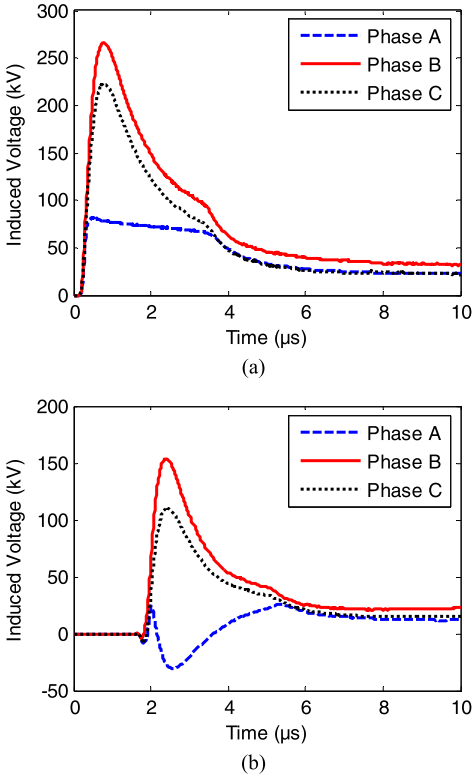

FIGURE 12. Voltage induced on the three-line conductors with MOA on phase A (σ=0.01S/m) (a) middle point, (b) termination.

VI. CONCLUSIONS

In this paper, a macro-model of Agrawal's field-to-line coupling model is proposed, which can be integrated into MATLAB/Simulink to evaluate LIOVs of overhead lines. In this model, the distributed equivalent voltage sources are lumped at the terminations of the lines. In order to interface

TABLE 3. Constant, residues and poles of Z_{ij}.

Z_{11}		Z_{22}		Z_{33}		Z_{12}		Z_{13}		Z_{23}	
R_{d11}		R_{d22}		R_{d33}		R_{d12}		R_{d13}		R_{d23}	
6.64×10^{2}		7.44×10^{2}		7.16×10^{2}		2.40×10^{3}		2.25×10^{3}		1.64×10^{3}	
r_{11}	p_{11}	r_{22}	p_{22}	r_{33}	p_{33}	r_{12}	p_{12}	r_{13}	p_{13}	r_{23}	p_{23}
4.20×10^{7}	-8.03×10^{5}	7.10×10^{7}	-1.11×10^{6}	5.32×10^{7}	-8.45×10^{5}	-1.40×10^{8}	-9.96×10^{5}	-2.35×10^{8}	-1.49×10^{6}	-1.29×10^{8}	-1.28×10^{6}
3.29×10^{6}	-4.86×10^{4}	8.51×10^{6}	-9.10×10^{4}	4.88×10^{6}	-5.63×10^{4}	-1.15×10^{7}	-6.85×10^{4}	-1.70×10^{7}	-1.03×10^{5}	-9.37×10^{6}	-8.50×10^{4}
1.82×10^{5}	-2.82×10^{3}	8.99×10^{5}	-8.84×10^{3}	3.67×10^{5}	-4.05×10^{3}	-4.80×10^{5}	-3.58×10^{3}	-6.16×10^{5}	-4.91×10^{3}	-3.67×10^{5}	-4.12×10^{3}
1.38×10^{4}	-9.75×10^{1}	1.00×10^{5}	-9.16×10^{2}	2.64×10^{4}	-2.85×10^{2}	9.89×10^{3}	-4.03×10^{1}	1.11×10^{4}	-4.37×10^{1}	1.24×10^{4}	-4.05×10^{1}
4.98×10^{3}	-1.31×10^{1}	4.98×10^{3}	-8.81×10^{0}	4.88×10^{3}	-1.42×10^{1}	5.43×10^{4}	-5.63×10^{0}	5.22×10^{4}	-5.50×10^{0}	4.04×10^{4}	-6.51×10^{0}
6.53×10^{3}	-1.47×10^{0}	5.75×10^{3}	-9.72×10^{-1}	6.92×10^{3}	-1.58×10^{0}	4.41×10^{4}	-7.32×10^{-1}	4.18×10^{4}	-7.07×10^{-1}	3.42×10^{4}	-8.76×10^{-1}

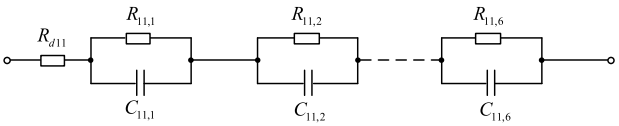

FIGURE 13. Equivalent circuit of Z_{11}.

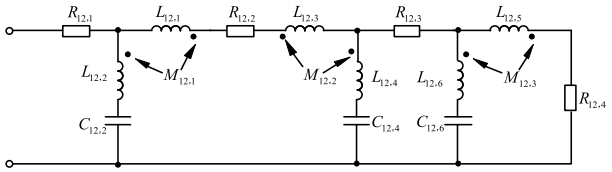

FIGURE 14. Equivalent circuit of Z_{12}.

with MATLAB/Simulink, the propagation function of MTLs is approximated by a delayed rational function and described by a state-space representation, and the Brune's synthesis is adopted to model the passive section in the macro-model in order to overcome the passivity violation problem. Furthermore, an ''early time model'' for the early time response is proposed to calculate the peak values of LIOVs, and the calculation of a LIOVs can be further simplified. Some examples are presented to demonstrate the accuracy of the proposed model, and the influence of the MOA and ground wire on the LIOVs are also discussed.

By using the proposed method, a complex network would be analyzed in future in order to achieve a rational protection.

APPENDIX

A. MODELLING OF THE PASSIVE SECTION OF MACRO-MODEL

The fitting parameters and corresponding equivalent circuits of Z_{ij} are described in detail in this section. The values of R_{dij}, r_{ij} and p_{ij} according to all the impedances in Fig. 1 are listed in Table 3. Considering that condition (17) is satisfied for the cases of $i = j$, Z_{ii} and can be modeled as Fig. 2. Taking Z_{11} as an example, its topology is shown in Fig. 13 and the values of the elements are list in Table 3. As for the cases of $i \neq j$, as can be seen from Table 3, some residues are negative, so condition (17) is not satisfied. Brune's synthesis is used to deal with the passivity violation problem. Taking Z_{12} as an example, its equivalent circuit is given in Fig. 14 and the parameters are listed in Table 4. In order to validate the equivalent circuits, the curves of the amplitude-frequency and the phase-frequency characteristics are shown in Fig. 15 and Fig. 16.

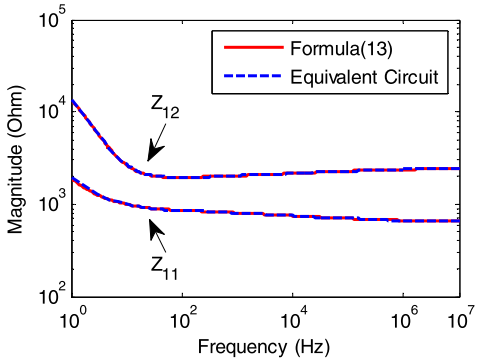

FIGURE 15. Amplitude-frequency characteristics of Z_{11} and Z_{12}.

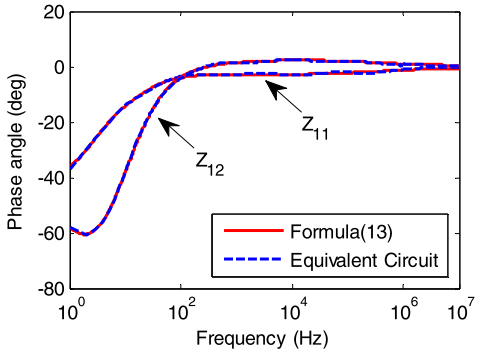

FIGURE 16. Phase-frequency characteristics of Z_{11} and Z_{12}.

B. EFFECTIVE LENGTH OF THE "EARLY TIME MODEL"

As we all know, the lightning striking distance presents a much broader rang, which will influence the rising times of LIOVs. In order to illustrate this problem, the peak values of LIOVs of different lightning striking distances are shown in Fig. 17. In these examples, the maximum lightning subsequent return-stroke current with 50kA peak value is considered and the maximum time-derivative is 200kA/μs [38], and the line configuration is same as example 1 in Section V.

TABLE 4. Parameters of the equivalent circuit of Z_{11} and Z_{12}.

UNIT: R:[Ω], C:[F], L:[H], M:[H]

Z_{11}						Z_{12}					
$R_{11,1}$	$R_{11,2}$	$R_{11,3}$	$R_{11,4}$	$R_{11,5}$	$R_{11,6}$	$R_{12,1}$	$R_{12,2}$	$R_{12,3}$	$C_{12,2}$	$C_{12,4}$	$C_{12,6}$
5.23×10^{1}	6.77×10^{1}	6.47×10^{1}	1.42×10^{2}	3.79×10^{2}	4.43×10^{3}	1.97×10^{3}	1.64×10^{4}	1.58×10^{4}	9.25×10^{-6}	3.58×10^{-6}	1.84×10^{-5}
$C_{11,1}$	$C_{11,2}$	$C_{11,3}$	$C_{11,4}$	$C_{11,5}$	$C_{11,6}$	$L_{12,1}$	$L_{12,2}$	$L_{12,3}$	$L_{12,4}$	$L_{12,5}$	$L_{12,6}$
2.38×10^{-8}	3.04×10^{-7}	5.49×10^{-6}	7.22×10^{-5}	2.01×10^{-5}	1.53×10^{-4}	3.48×10^{0}	3.82×10^{-2}	2.07×10^{-3}	2.32×10^{-1}	8.91×10^{-3}	1.19×10^{-2}
R_{d11}						$M_{12,1}$	$M_{12,2}$	$M_{12,3}$			
6.64×10^{2}						3.65×10^{-1}	2.19×10^{-2}	1.03×10^{-2}			

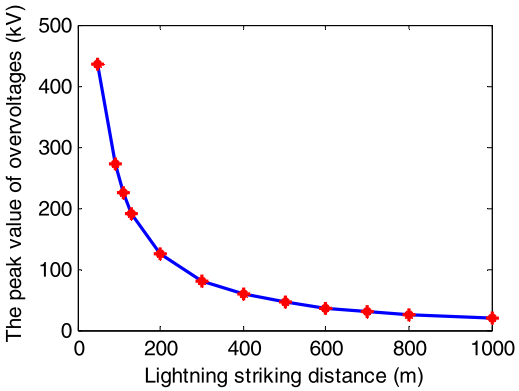

FIGURE 17. The peak values of lightning induced voltages of the different lightning striking distances.

TABLE 5. The rising time of LIOVs about different lightning striking distances.

Lightning striking distance/m	50	90	200	300	400
Rising time of LIOVs/μs	0.70	0.80	1.20	1.65	2.00

As can be seen from Fig. 17, when the lightning striking distance is larger than 400m, it would not cause an insulation flashover, and the corresponding rising times at different lightning striking distances are listed in Table 5, in which the rising time of LIOVs is about $1\sim2\mu$s. On the other hand, as for a line longer than 500m, the time delay from one end to other would be greater than $2\mu s$, which is longer than the rising time of LIOVs. It can be imagined that the LIOVs would not be influenced by the current sources $\boldsymbol{I}_s(x_1)$ and $\boldsymbol{I}_s(x_2)$ in Fig. 1 which is related to the reflections from the other end. As a result, Fig.1 can be simplified to Fig. 3 when the length of the line is longer than 500m.

Finally, considering that the front time of lightning presents a much broader rang, such as the first return-stroke current whose front time is longer than the subsequent return-stroke current, the rising time of LIOVs will be also longer and the effective length of the line should be adjusted accordingly. Given that the calculation of the LIOVs is usually discussed under a subsequent return-stroke current, which is also the focus of this paper. As the statements above, as for a line longer than 500m, the effective length of the 'early time model' is adopted as 500m.

REFERENCES

[1] P. N. Mikropoulos and T. E. Tsovilis, "Statistical method for the evaluation of the lightning performance of overhead distribution lines," *IEEE Trans. Dielectr. Electr. Insul.*, vol. 20, no. 1, pp. 202–211, Feb. 2013.

[2] T. H. Thang, Y. Baba, A. Piantini, and V. A. Rakov, "Lightning-induced voltages in the presence of nearby buildings: FDTD simulation versus small-scale experiment," *IEEE Trans. Electromagn. Compat.*, vol. 57, no. 6, pp. 1601–1607, Dec. 2015.

[3] X. Liu, X. Cui, and L. Qi, "Time-domain finite-element method for the transient response of multiconductor transmission lines excited by an electromagnetic field," *IEEE Trans. Electromagn. Compat.*, vol. 53, no. 2, pp. 462–474, May 2011.

[4] C. R. Paul, "The general solution for an (n+1)-conductor line," in *Analysis of Multiconductor Transmission Lines*, vol. 21, 2nd ed. New York, NY, USA: Wiley, 2008, ch. 7, pp. 282–342,

[5] F. M. Tesche and C. M. Butler, "On the addition of EM field propagation and coupling effects in the BLT equation," Kirtland Air Force Base, Albuquerque, NM, USA, Interact. Note 588, Dec. 2003.

[6] F. M. Tesche, "Development and use of the BLT equation in the time domain as applied to a coaxial cable," *IEEE Trans. Electromagn. Compat.*, vol. 49, no. 1, pp. 3–11, Feb. 2007.

[7] C. E. Baum, T. K. Liu, and F. M. Tesche, "On the analysis of general multiconductor transmission line networks," Kirtland, AFB, NM, USDA, Interact. Note 350, Nov. 1978.

[8] C. A. Nucci, F. Rachidi, M. V. Ianoz, and C. Mazzetti, "Lightning-induced voltages on overhead lines," *IEEE Trans. Electromagn. Compat.*, vol. 35, no. 1, pp. 75–86, Feb. 1993.

[9] F. Rachidi, "A review of field-to-transmission line coupling models with special emphasis to lightning-induced voltages on overhead lines," *IEEE Trans. Electromagn. Compat.*, vol. 54, no. 4, pp. 898–911, Aug. 2012.

[10] J. O. S. Paulino, C. F. Barbosa, I. J. da Silva Lopes, and G. C. de Miranda, "Time-domain analysis of rocket-triggered lightning-induced surges on an overhead line," *IEEE Trans. Electromagn. Compat.*, vol. 51, no. 3, pp. 725–732, Aug. 2009.

[11] C. F. Barbosa and J. O. S. Paulino, "An approximate time-domain formula for the calculation of the horizontal electric field from lightning," *IEEE Trans. Electromagn. Compat.*, vol. 49, no. 3, pp. 593–601, Aug. 2007.

[12] R. Montano, N. Theethayi, and V. Cooray, "An efficient implementation of the Agrawal model for lightning-induced voltage calculations using circuit simulation software," *IEEE Trans. Circuits Syst. I, Reg. Papers*, vol. 55, no. 9, pp. 2959–2965, Oct. 2008.

[13] G. S. Shinh, N. M. Nakhla, R. Achar, M. S. Nakhla, A. Dounavis, and I. Erdin, "Fast transient analysis of incident field coupling to multiconductor transmission lines," *IEEE Trans. Electromagn. Compat.*, vol. 48, no. 1, pp. 57–73, Feb. 2006.

[14] H. Xie, J. Wang, R. Fan, and Y. C. Liu, "Application of a SPICE model for multiconductor transmission lines in electromagnetic topology," in *Proc. PIRES*, 2008, pp. 237–241.

[15] H. K. Høidalen, "Calculation of lightning-induced overvoltages using MODELS," in *Proc. Int. Conf. Power Syst. Transient*, Budapest, Hungary, 1999, pp. 359–364.

[16] H. K.Høidalen, "Calculation of lightning-induced voltages in MODELS including lossy ground effects," in *Proc. Int. Conf. Power Syst. Transient*, New Orleans, LA, USA, 2003, pp. 1–6.

[17] A. Borghetti, J. A. Gutierrez, C. A. Nucci, M. Paolone, E. Petrache, and F. Rachidi, "Lightning-induced voltages on complex distribution systems: Models, advanced software tools and experimental validation," *J. Electrostatics*, vol. 60, pp. 163–174, Mar. 2004.

[18] F. Napolitano, A. Borghetti, C. A. Nucci, M. Paolone, F. Rachidi, and J. Mahserejian, "An advanced interface between the LIOV code and the EMTP-RV," in *Proc. 29th Int. Conf. Lightning Protection*, Uppsala, Sweden, 2008, pp. 1–12.
[19] A. Andreotti, A. Pierno, and V. A. Rakov, "A new tool for calculation of lightning-induced voltages in power systems—Part I: Development of circuit model," *IEEE Trans. Power Del.*, vol. 30, no. 1, pp. 326–333, Feb. 2015.
[20] A. Andreotti, A. Pierno, and V. A. Rakov, "A new tool for calculation of lightning-induced voltages in power systems—Part II: Validation study," *IEEE Trans. Power Del.*, vol. 30, no. 1, pp. 334–341, Feb. 2015.
[21] A. Maffucci and G. Miano, "An accurate time-domain model of transmission lines with frequency-dependent parameters," *Int. J. Circuit Theory Appl.*, vol. 28, no. 3, pp. 263–280, May 2000.
[22] X. Liu, X. Cui, and L. Qi, "Calculation of lightning-induced overvoltages on overhead lines based on DEPACT macromodel using circuit simulation software," *IEEE Trans. Electromagn. Compat.*, vol. 54, no. 4, pp. 837–849, Aug. 2012.
[23] B. Gustavsen and A. Semlyen, "Rational approximation of frequency domain responses by vector fitting," *IEEE Trans. Power Del.*, vol. 14, no. 3, pp. 1052–1061, Jul. 1999.
[24] E. Richards, "Applications of vector fitting in the solution of electromagnetic field interactions," Ph.D. dissertation, Dept. Elect. Eng., Univ. Arizona State, Tempe, AZ, USA, 2014.
[25] O. Brune, "Synthesis of a finite two-terminal network whose driving-point impedance is a prescribed function of frequency," Ph.D dissertation, Dept. Elect. Eng., Massachusetts Inst. Technol., Cambridge, MA, USA, 2010.
[26] F. Rachidi, C. A. Nucci, M. Ianoz, and C. Mazzetti, "Influence of a lossy ground on lightning-induced voltages on overhead lines," *IEEE Trans. Electromagn. Compat.*, vol. 38, no. 3, pp. 250–264, Aug. 1996.
[27] Z. Qi, H. Yu, P. Liu, S. X.-D. Tan, and L. He, "Wideband passive multiport model order reduction and realization of RLCM circuits," *IEEE Trans. Comput.-Aided Des. Integr. Circuits Syst.*, vol. CAD-25, no. 8, pp. 1496–1509, Aug. 2006.
[28] O. Brune, "Synthesis of a finite two-terminal network whose driving-point impedance is a prescribed function of frequency," *J. Math. Phys.*, vol. 10, nos. 1–4, pp. 191–236, 1931.
[29] B. Gustavsen, "Optimal time delay extraction for transmission line modeling," *IEEE Trans. Power Del.*, vol. 32, no. 1, pp. 45–54, Feb. 2017.
[30] B. Gustavsen and A. Semlyen, "Simulation of transmission line transients using vector fitting and modal decomposition," *IEEE Trans. Power Del.*, vol. 13, no. 2, pp. 605–614, Apr. 1998.
[31] O. Ramos-Leaños, J. L. Naredo, and J. A. Gutierrez-Robles, "An advanced transmission line and cable model in Matlab for the simulation of power-system transients," in *MATLAB: A Fundamental Tool for Scientific Computing and Engineering Applications*, 1st ed. Rijeka, Croatia: InTech, 2012, Ch. 12, pp. 269–304.
[32] X. Liu, J. Yang, G. Liang, and L. Wang, "Modified field-to-line coupling model for simulating the corona effect on the lightning induced voltages of multi-conductor transmission lines over a lossy ground," *IET, Gener., Transmiss., Distrib.*, vol. 11, no. 7, pp. 1865–1876, Jun. 2017.
[33] F. Delfino, R. Procopio, M. Rossi, F. Rachidi, and C. A. Nucci, "Lightning return stroke current radiation in presence of a conducting ground: 2. Validity assessment of simplified approaches," *J. Geophys. Res.*, vol. 113, no. D5, pp. D05111-1–D05111-11, 2008.
[34] V. Cooray, "Horizontal fields generated by return strokes," *Radio Sci.*, vol. 27, no. 4, pp. 529–537, Jul./Aug. 1992.
[35] M. Rubinstein, "An approximate formula for the calculation of the horizontal electric field from lightning at close, intermediate, and long range," *IEEE Trans. Electromagn. Compat.*, vol. 38, no. 3, pp. 531–535, Aug. 1996.
[36] J. Zou, B. Zhang, X. Du, J. Lee, and M. Ju, "High-efficient evaluation of the lightning electromagnetic radiation over a horizontally multilayered conducting ground with a new complex integration path," *IEEE Trans. Electromagn. Compat.*, vol. 56, no. 3, pp. 659–667, Jun. 2014.
[37] Y. Baba and V. A. Rakov, "Voltages induced on an overhead wire by lightning strikes to a nearby tall grounded object," *IEEE Trans. Electromagn. Compat.*, vol. 48, no. 1, pp. 212–224, Feb. 2006.
[38] *Protection Against Lightning—Part 1: General Principles*, Standard IEC 62305-1:2010, North China Electr. Power Univ., Tianjin, China, 1980.

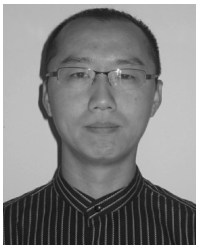

XIN LIU was born in Tianjin, China, in 1980. He received the B.S. degree from North China Electric Power University (NCEPU), Baoding, Hebei, China, in 2003, the M.S. degree from the Huazhong University of Science and Technology, Wuhan, Hubei, China, in 2006, and the Ph.D. degree from NCEPU, Beijing, China, in 2013, respectively.

He is currently an Associate Professor with the Department of Electrical Engineering, NCEPU. His research interests include electromagnetic pulse interaction with transmission lines, electromagnetic compatibility on power systems, and high-voltage equipment modeling.

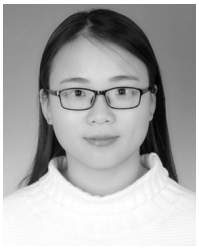

ZIWEI FAN was born in Hebei, China, in 1993. She received the B.S. degree from the Hebei University of Architecture, Hebei, in 2016.

She is currently pursuing the M.S. degree in electrical engineering with North China Electric Power University, Hebei. Her research interests include electromagnetic pulse interaction with transmission lines and electromagnetic compatibility on power systems.

GUISHU LIANG was born in Shijiazhuang, Hebei, China, in 1961. He received the B.S., M.S., and Ph.D. degrees in electrical engineering from North China Electric Power University (NCEPU), Baoding, Hebei, China, in 1982, 1987, and 2008, respectively.

He is currently a Professor and the Head of the Electrical Theory Research Office, NCEPU. His current research interests include the application of electrical network theory in power systems and electromagnetic compatibility on power systems.

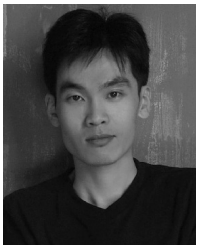

TAO WANG was born in Baoding, Hebei, China, in 1975. He received the B.S. and M.S. degrees in electrical engineering from North China Electric Power University (NCEPU), Baoding, in 1997 and 2004, respectively.

He is currently a Lecturer with the Department of Electrical Engineering, NCEPU. His current research interests include the application of electrical network theory in power systems and electromagnetic compatibility on power systems.